Available online at www.sciencedirect.com
ScienceDirect
Polymer 48 (2007) 356–362
polymer
www.elsevier.com/locate/polymer

Fractionated crystallization in PA6/ABS blends: Influence of a reactive compatibilizer and multiwall carbon nanotubes

Suryasarathi Bose [a], Arup R. Bhattacharyya [a,*], Pravin V. Kodgire [b], Ashok Misra [b,1]

[a] Department of Metallurgical Engineering and Materials Science, Indian Institute of Technology Bombay, Powai, Mumbai 400076, Maharashtra, India
[b] Department of Chemical Engineering, Indian Institute of Technology Bombay, Powai, Mumbai 400076, Maharashtra, India

Received 19 June 2006; received in revised form 6 November 2006; accepted 12 November 2006
Available online 30 November 2006

Abstract

The 20/80 blends of polyamide 6 (PA6) and acrylonitrile–butadiene–styrene copolymer (ABS) in the presence of styrene–maleic anhydride copolymer (SMA) and multiwall carbon nanotubes (MWNT) were prepared using melt-mixing technique. Crystallization behavior of the PA6 phase in the blends was studied using DSC, WAXD and SAXS techniques. Blends' morphology was characterized by SEM. We observed fractionated crystallization of PA6 phase in 20/80 PA6/ABS blends. It was also observed that the phenomenon of fractionated crystallization was influenced by the presence of both SMA and MWNT. Blends' morphology revealed the presence of wide domain size distribution of PA6 droplets in the amorphous ABS matrix. On incorporation of either SMA or SMA modified MWNT, the average domain size of PA6 droplets was found to be finer up to 1 wt% SMA modified MWNT. Encapsulation of SMA copolymer layer on the MWNT surface was also evident from SEM micrographs. SAXS analysis revealed the formation of multiple lamellae stacking of PA6 phase in the presence or absence of SMA and MWNT in 20/80 PA6/ABS blends. This was attributed to the formation of less perfect crystallites formed during the cooling of melt at higher degree of supercooling.

Keywords: PA6/ABS blends; Multiwall carbon nanotubes; Fractionated crystallization

1. Introduction

Blending of immiscible polymers is one of the most efficient ways to obtain polymeric materials with specific beneficial properties. In many of these blends a semi-crystalline component is dispersed as minor phase into a matrix of another component. Usually when blended with additional components, numerous new interfaces are introduced between the additional components and the crystalline matrix. The area of the interface depends on the components and the distribution of additional components in the crystalline matrix. However, not all the interfaces can play a role as nucleation centers. For immiscible and incompatible blends, since their interfacial tension is higher and the interface between them is very sharp, the thickness of their interfacial layer is very small. Thus, interface which wets well with the crystalline matrix can cause heterogeneous nucleation [1,2]. However, if the crystallizable polymer exists as a minor phase and dispersed as droplets in an immiscible matrix then instead of crystallizing at their bulk crystallization temperature, a series of crystallization exotherms are found to appear at much lower temperatures; the phenomenon is often referred as fractionated crystallization [3]. In this case the existing heterogeneities are subdivided into isolated regions (usually as droplets) and the number is significantly greater than the number of usual active heterogeneities at lower supercooling. When such dispersion is cooled from the melt, a series of crystallization exotherms can be observed. This phenomenon has been observed in a series of immiscible blend systems which include iPP/PA6 [4,5],

* Corresponding author. Tel.: +91 22 25767634; fax: +91 22 25723480.
E-mail address: arupranjan@iitb.ac.in (A.R. Bhattacharyya).
[1] Director, Indian Institute of Technology Bombay, Powai, Mumbai 400076, Maharashtra, India.

0032-3861/$ - see front matter © 2006 Elsevier Ltd. All rights reserved.
doi:10.1016/j.polymer.2006.11.019

EPDM/PA6 [6], PVDF/PA6 [3,7], (PPE/PS)/PA6 [8], PPE/PA6 [8], SPS/PA6 [9], PP/PA12 [10], LDPE/PA6 [11], PS/PA6 [12], PP/mPA [13], PTFE/PA [14], (PPE/PS)/PA6 [15], PPE/PA6 [16], ABS/PA6.10 [17], PP/PP-*g*-MAH/PA6 [18].

After an extensive survey of the earlier investigations [3–18] in this regard, we found that fractionated crystallization was strongly influenced by either of the following: (1) type and the amount of the compatibilizer; (2) addition of a nucleating agent; (3) domain size and distribution of the dispersed phase; (4) polymorphism of the dispersed phase; and (5) processing parameters during melt-mixing. Though the earlier reports carried the information of the individual role of a compatibilizer or a nucleating agent affecting the fractionated crystallization, the combined effect of a compatibilizer and a nucleating agent in an immiscible blend system did not receive much attention. Hence, it is our focus to get insight of this phenomenon in a filled compatibilized blend system with filler acting as a nucleating agent.

One such immiscible blend system, we found of significant commercial and academic interest is blends of polyamide 6 (PA6) and copolymer of acrylonitrile–butadiene–styrene (ABS). In the development of these blends the concept of reactive compatibilization and the use of styrene–maleic anhydride copolymer (SMA) as an effective compatibilizer was described extensively in the past [19–22].

Since the discovery of carbon nanotubes (CNTs) by Iijima [23], CNTs have emerged as a potential candidate as filler in polymer based composites due to their unique mechanical, electrical and thermal properties. Earlier literatures showed the potential of CNTs as nucleating agent, which strongly affect the crystallization behavior of the semi-crystalline polymer [24–28]. Thus, it motivated us to study the crystallization behavior of PA6/ABS blend system in the presence of SMA and multiwall carbon nanotubes (MWNT) using differential scanning calorimetry (DSC), wide-angle X-ray diffraction (WAXD) and small-angle X-ray scattering (SAXS) techniques. Morphological characterization was carried out by scanning electron microscopy (SEM).

2. Experimental

2.1. Materials and specimen preparations

Polyamide 6 (PA6) with a zero shear viscosity of 179.2 Pa s at 260 °C was obtained from GSFC, Gujarat, India (Gujlon M28RC, relative viscosity 2.8, M_v is 38 642 in 85% formic acid). Acrylonitrile–butadiene–styrene (ABS) copolymer (Absolac-120) was supplied by Bayer India Ltd. Styrene–maleic anhydride copolymer (SMA) with 8% MA content (Dylark 232) was supplied by Nova Chemicals, USA. Multiwall carbon nanotubes (MWNT) were obtained from Iljin Nanotech, Korea, which were synthesized by CVD technique of purity level >90% (length = 10–50 μm, diameter = 10–20 nm). The 20/80 PA6/ABS blends were prepared by melt-mixing in a conical twin-screw extruder (Micro 5, DSM Research, Netherlands) at 260 °C with a rotational speed of 150 rpm for 5 min. Preblended SMA and MWNT of 95:5 ratio (here after assigned as SMA modified MWNT denoted by 'M') were used as a compatibilizer and prepared by melt-mixing under the same extrusion conditions. The blend compositions with their sample codes are listed in Table 1. Prior to mixing, the materials were dried for 24 h at 80 °C in a vacuum oven. Compression molded films with 0.5 mm thickness were prepared at 260 °C.

Table 1
Sample code and composition of blends of PA6/ABS with and without SMA modified MWNT

Sample code	PA6 (wt%)	ABS (wt%)	SMA (wt%)	MWNT (wt%)
N6	100	–	–	–
N20A80	20	80	–	–
N20A80S2	19.6	78.4	2	–
N20A80M0.5	19.9	79.6	0.475	0.025
N20A80M1	19.8	79.2	0.95	0.05
N20A80M2	19.6	78.4	1.9	0.1
N20A80M5	19	76	4.75	0.25
N20A80T1	19.8	79.2	–	1

M denotes a preblend of SMA copolymer and MWNT in 95:5 weight ratio and T indicates MWNT.

2.2. Characterization

Differential scanning calorimetric (DSC) measurements were carried out in Perkin–Elmer DSC-6 using Pyris software. The extruded samples of about 5 mg were dried in a vacuum oven prior to experiment. The heating–cooling–heating cycles were recorded in the temperature range from 10 °C to 260 °C at a scan rate of ±10 K/min under nitrogen atmosphere. Temperature and heat transition were calibrated with indium standard. In the first heating run all samples were annealed at the final temperature (260 °C) for 3 min to delete the previous thermal history. The degree of crystallinity of PA6 phase was calculated from the heat of fusion of second heating cycle. The heat of fusion (ΔH_m) of PA6 phase was normalized to the fraction of polymer present in the blends. The degree of crystallinity (X_c) of PA6 phase was determined from the ratio of normalized heat of fusion ($\Delta H_{m,norm}$) to the heat of fusion of 100% crystalline PA6, $(\Delta H_m)_0$, which was taken as 204.8 J/g [29].

Wide-angle X-ray diffraction (WAXD) studies were carried out on a Philips X-Pert Pro. The incident X-rays (λ=1.54 Å) from the Cu-target were monochromatized using a Ni filter. Compression molded samples of 0.5 mm thickness were used as test specimens. WAXD patterns were recorded with a step scan with step size of 0.02 between 5° and 40° 2θ.

Small-angle X-ray scattering (SAXS) experiments were performed with line collimation geometry, using SAXSess camera (Anton Paar GmbH). The Cu Kα incident radiation from PANalytical X-ray source at 40 kV (40 mA) was used. Samples were kept in between the copper plates for 15 min. Image plate reader (Packard Bioscience, Inc) was used to record the scattering and the images were generated by software: OptiQuant (Packard Bioscience, Inc). The SAXSquant produces one-dimensional scattering curves by averaging two-dimensional scattering patterns over linear or circular paths.

Scanning electron microscopy (SEM) was performed using FEI Quanta 200 with gold sputtering on the etched surface. The extruded strands were cryo-fractured using liquid nitrogen and etched in formic acid in order to remove the PA6 phase of the blends. The weight-average diameter (D_w) of the PA6 droplets was calculated using the following equation:

$$D_w = \left(\sum n_i d_i^2\right) \Big/ \left(\sum n_i d_i\right)$$

where n_i indicates the number of droplets having d_i as their diameter.

3. Results and discussion

The cooling scans of PA6/ABS blends with and without SMA and MWNT are presented in Fig. 1a. It is to be noted that the bulk crystallization temperature (T_c) of pure PA6 is observed at ~192.8 °C and is excluded from Fig. 1a in order to magnify the crystallization exotherm signals from PA6, which is dispersed as minor component. The cooling scan of the PA6 phase in the 20/80 PA6/ABS blends exhibits a crystallization exotherm at ~184.3 °C (here after termed as first crystallization temperature) and weak exotherms at ~160.3 °C (here after termed as second crystallization exotherm) and at ~112.3 °C (here after termed as third crystallization exotherm).

According to Turnbull's approximate relation [30]

$$T_{c,hom} = 0.8T_E$$

where $T_{c,hom}$ is the crystallization temperature induced by homogeneous nucleation and T_E is the melt/crystallization equilibrium temperature. According to the above empirical equation, $T_{c,hom}$ for PA6 is found to be ~120 °C. The lowest observable exotherm in 20/80 PA6/ABS blends is found at ~112.3 °C (Fig. 1a), which can be attributed to the homogeneous crystallization of PA6. The other crystallization exotherms may be the result of heterogeneously nucleated droplets. It is believed that wider domain size distribution of PA6 droplets is related to the different heterogeneities active at specific undercooling, which will be discussed under the morphological analysis [31–33].

Further, it is clearly observed that the crystallization behavior of PA6 is strongly affected in the presence of ABS. A delay in crystallization process is observed in the 20/80 blend where the first crystallization temperature is ~8 °C lower than the bulk crystallization temperature of PA6. It is to be noted that lowering the crystallization temperature indicates migration of the heterogeneities from the crystallizable phase during melt-mixing [31–33], which again depends on the viscosity ratio of melt. It is reported that lower the melt-viscosity ratio of the blend, the finer the average droplet size of the dispersed phase. The droplet size of the dispersed phase varies from 0.08 μm to 4 μm in 20/80 PA6/ABS blends (see morphological analysis). It is observed that larger droplets that contain the heterogeneities are usually active at lower supercooling and will crystallize at temperature (~184.3 °C) corresponding to the bulk crystallization temperature of PA6. Smaller droplets, which contain other types of less efficient heterogeneities, will nucleate at the supercooling that is necessary for those heterogeneities to become active (~160.3 °C). Finally, the smallest droplets that do not contain any heterogeneity are forced to crystallize homogeneously (~112.3 °C).

On addition of 2 wt% SMA to the blend, the first crystallization exotherm (Fig. 1(a)) is found to appear at ~184.3 °C indicating a delay in the crystallization process of PA6 and subsequent homogeneous crystallization of PA6 is found at ~112.3 °C. Moreover, the weak exotherm at ~160.3 °C is found to be absent indicating the suppression of this crystallization exotherm at this temperature. It seems that either the concentration of SMA or its effectiveness as a compatibilizer is insufficient to aid finer degree of dispersion leading to heterogeneities, which are active at ~184.3 °C and ~112.3 °C.

The second crystallization exotherm again reappeared in the blends on addition of 0.5 wt% SMA modified MWNT. This clearly indicates that the concentration of SMA and SMA modified MWNT content in the blend plays a key role in governing the fractionated crystallization phenomenon.

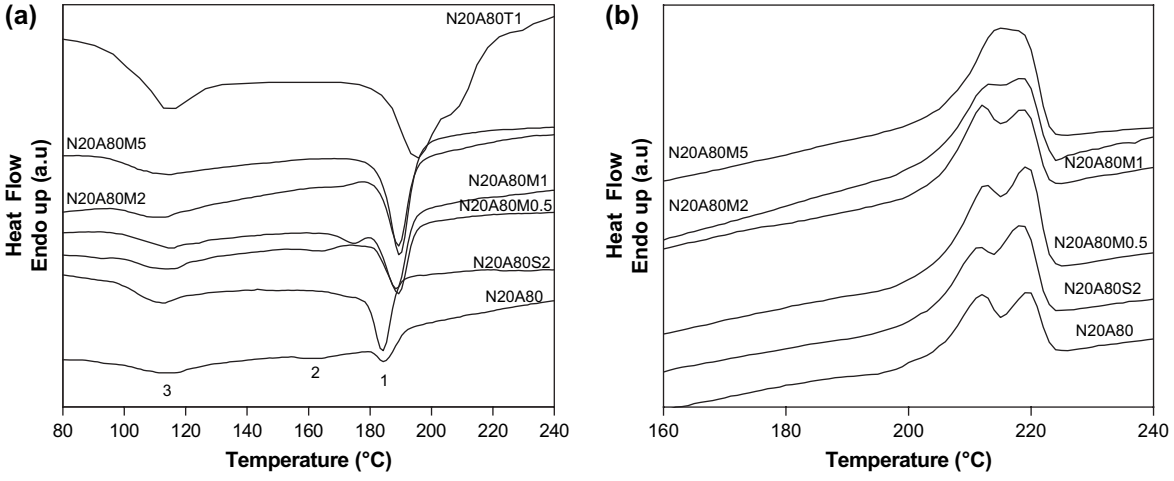

Fig. 1. DSC: (a) cooling and (b) second heating scans of blends of PA6/ABS with and without SMA modified MWNT.

On incorporation of 0.5 wt% SMA modified MWNT in the blend a significant change in the first crystallization exotherm is observed, at ~189.3 °C, though it is still lower than the bulk crystallization temperature of the PA6 phase indicating the persistent delay in the crystallization process. However, the increase in the crystallization temperature as compared to uncompatibilized and SMA compatibilized blends indicates heterogeneous nucleation from the MWNT. It is also to be noted that the second crystallization exotherm is also shifted towards smaller degree of supercooling. In the case of the blends filled with 0.5 wt% of SMA modified MWNT, the second crystallization exotherm is observed at 163.3 °C which later shifted towards smaller degree of supercooling as the content of SMA modified MWNT increases from 0.5 wt% to 2 wt%. However, this crystallization exotherm is found to be absent again in the case of blends filled with 5 wt% SMA modified MWNT indicating suppression of crystallization at this temperature in the presence of SMA modified MWNT. It is appeared that the increasing concentration of SMA in the blends leads to the finer size distribution of PA6 droplets as compared to the uncompatibilized PA6/ABS blends, which is responsible for generating heterogeneities active at specific supercooling. However, it can also be commented that the effectiveness of the compatibilizer is insufficient to produce sub-micron size droplets in all the blends (see morphological analysis). On the contrary, MWNT are providing heteronucleation sites which is reflected by the increase in crystallization temperatures. The fact, which still remains unclear, is why there is no further change in the first crystallization exotherm with increasing MWNT content? It hints at some hindrance to the nucleation/crystal growth process from the heterogeneous site as would have been provided by the MWNT. These observations will be discussed while studying the morphology of the blend systems. In order to detect the individual role of MWNT in the fractionated crystallization process, it was necessary to study the crystallization process of the blend in the absence of SMA. Hence, we have carried out crystallization studies with 20/80 PA6/ABS blends filled with 1 wt% MWNT. Surprisingly, the second crystallization exotherm is completely suppressed and a strong crystallization exotherm is obtained at ~195.7 °C, well above the bulk crystallization temperature of PA6. Moreover, the third crystallization temperature ($T_{c,hom}$) was recorded at ~116.8 °C, which is drastically shifted towards the lower degree of supercooling in the presence of MWNT indicating the heterogeneous nucleation sites provided by MWNT. Hence, it is worthy to mention that both compatibilizer and filler content play a crucial role in governing the fractionated crystallization phenomenon.

DSC melting endotherms (Fig. 1b) indicate that PA6 (not shown here) and the different blend compositions of 20/80 PA6/ABS show double melting endotherms during the second heating cycle. In the presence of 5 wt% SMA modified MWNT, we observed single melting endotherm with broadening. The presence of double melting endotherms may be due to the different crystalline forms of PA6 or may be due to a process related to melting–recrystallization during heating. The occurrence of double melting endotherms of PA6 phase has been explained in the subsequent section while dealing with wide-angle X-ray diffraction (WAXD) analysis. It is also evident from Table 2 that percent crystallinity (X_c) of PA6 phase decreases in the uncompatibilized and SMA compatibilized 20/80 PA6/ABS blends. It is further observed from Table 2 that on incorporation of SMA modified MWNT, X_c is found to increase as compared to uncompatibilized blends, which may be due to the heterogeneous nucleation provided by the MWNT.

Table 2
DSC melting and crystallization parameters for PA6 and blends of PA6/ABS with and without SMA modified MWNT

Sample code	T_m	T_c	X_c (%)
N6	216.9, 220.9	192.1	34.8
N20A80	211.8, 219.4	184.3, 160.3, 112.3	23
N20A80S2	211.4, 217.6	184.3, 112.3	22.7
N20A80M0.5	212.5, 219.0	189.3, 163.3, 112.3	28.8
N20A80M1	211.9, 218.8	189.3, 175.3, 112.3	29.8
N20A80M2	211.9, 218	189.3, 171.3, 112.3	30.9
N20A80M5	214.7	189.3, 112.3	36

Fig. 2 depicts the WAXD pattern for 20/80 PA6/ABS blends in the presence and absence of SMA modified MWNT. Two sharp diffraction maxima at 2θ values of 20.1° and 23.6° are observed in the diffraction pattern corresponding to the d spacings of 4.41 and 3.76 Å which corresponds to α-crystalline (monoclinic) form of PA6. Peak at 20.1° corresponds to plane (200) and peak at 23.6° corresponds to planes (002) and (202). Peak at 21.5° was also observed, showing the presence of metastable γ-form (pseudohexagonal) of PA6. This peak corresponds to the (001) plane. It is also observed that the d spacings remain unaltered in the case of uncompatibilized blends and with SMA modified MWNT addition. Interestingly, addition of 1 wt% MWNT in 20/80 PA6/ABS blends resulted in significant changes in the ratio of α/γ

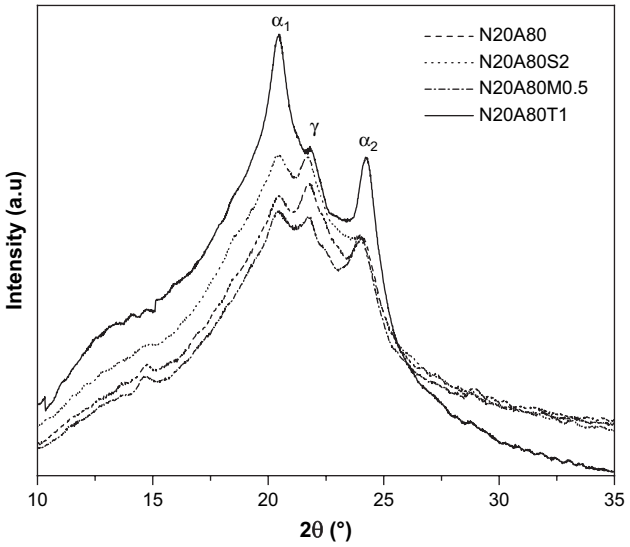

Fig. 2. WAXD patterns of blends of PA6/ABS with and without SMA modified MWNT.

crystalline forms of PA6, which is evident in Fig. 2. This observation indicates that in the presence of 1 wt% MWNT α-crystalline form of PA6 dominates over metastable γ-form. It is to be pointed out that the occurrence of double melting endotherms of PA6 in DSC studies may be related to the presence of both α-crystalline and metastable γ-form of PA6. Since pure PA6 also showed the presence of α and γ crystalline forms, it was not possible to comment on any correlation between the polymorphism phenomenon of PA6 and the fractionated crystallization behavior of 20/80 PA6/ABS blends.

Fig. 3a shows plot of intensity (I) versus scattering vector (q) of SAXS profile of 20/80 PA6/ABS blends. Fig. 3b shows the Lorentz corrected SAXS profile (Iq^2 versus q curve) of 20/80 PA6/ABS blends in the presence and absence of SMA modified MWNT. The inset of Fig. 3b compares the Iq^2 versus q plot of pure PA6 and 20/80 blends of PA6/ABS filled with 1 wt% MWNT. It is observed from the inset of Fig. 3b that pure PA6 shows periodicity of alternating crystalline lamellae and amorphous interlayer which is manifested in a scattering maxima corresponding to $q = 0.6\ \mathrm{nm}^{-1}$ and the long period is found to be 94.4 Å. Several scattering maxima at different q regions are observed for 20/80 PA6/ABS blends (Fig. 3b), which are related to the multiple lamellae stacking of different crystals activated at different supercooling. It is also observed that 20/80 PA6/ABS blends exhibit scattering maxima corresponding to pure PA6 in the range $0.2 < q < 0.7$ with several other scattering maxima in the higher q region ($0.7 < q < 1.0$; $1.0 < q < 1.2$; $1.2 < q < 1.4$). This implies that the long period or the corresponding crystalline lamella thickness (L_c) at higher q region is much lower as compared to pure PA6. A decrease in L_c indicates the formation of imperfect crystallites from the melt. This observation is found to be consistent with either SMA incorporated or SMA modified MWNT added PA6/ABS blends. However, the effects of SMA or SMA modified MWNT on fractionated crystallization of PA6 were not possible to distinguish from the SAXS pattern.

SEM micrographs of different set of blends can be found from Fig. 4. The blend samples were selectively etched by formic acid to remove the PA6 phase (as ABS did not swell or dissolve in formic acid). On an average 200 droplets and three micrographs of different magnifications were considered to evaluate the weight-average diameter (D_w) of the droplets. A wider distribution of PA6 droplets (D_w is 2.27 μm) can be found in Fig. 4a for uncompatibilized 20/80 PA6/ABS blends. The role of SMA, as a compatibilizer, in decreasing the domain size (D_w is 1.4 μm) is evident in Fig. 4b for 2 wt% SMA compatibilized PA6/ABS blends. On addition of 0.5 wt% SMA modified MWNT, D_w is found to be 0.89 μm (Fig. 4c). The observation of decreasing domain size is found to be consistent with increasing SMA modified MWNT concentration of up to 1 wt% SMA modified MWNT content (Fig. 4d and e; $D_w = 0.74$ μm and 1.85 μm at 1 wt% and 2 wt% SMA modified MWNT, respectively). A different kind of morphology is seen in the case of blends filled with 5 wt% SMA modified MWNT. This may be due to strong melt interfacial reaction between the anhydride groups of the SMA copolymer and the amine end groups of the PA6 phase. However, the effectiveness of the compatibilizer is insufficient to produce sub-micron size droplets in all the blends. Further, encapsulation of MWNT by the SMA copolymer can be seen (Fig. 5) in this set of blends, which is manifested with differences in the diameter of encapsulated MWNT. The encapsulating SMA copolymer layer thereby hinders the nucleation and subsequent crystal growth from the heterogeneity site as would have been provided by the MWNT. However, both the SMA and the MWNT content are crucial in governing the fractionated crystallization phenomenon in these blend system.

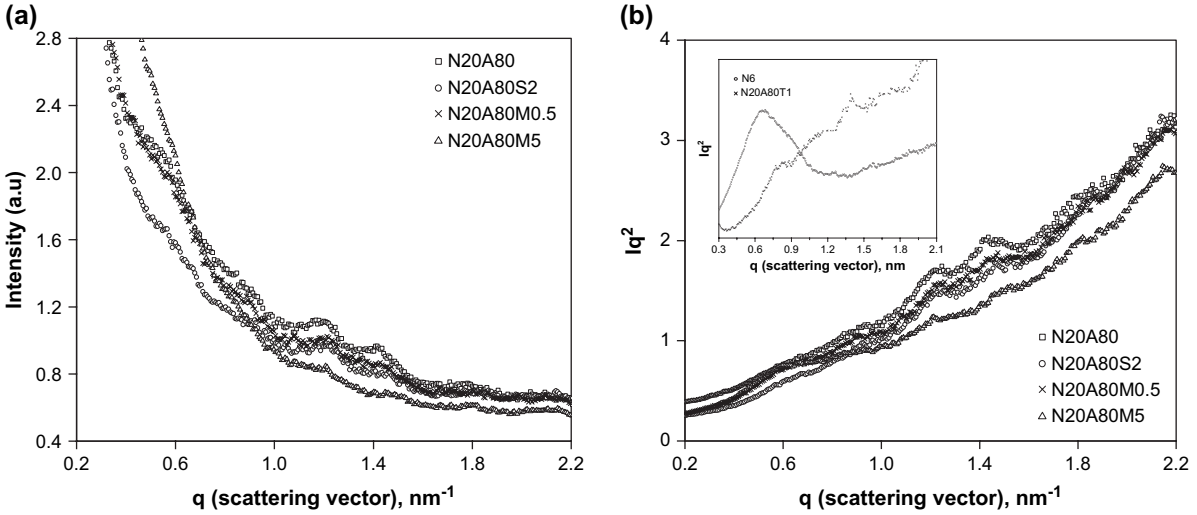

Fig. 3. SAXS pattern of (a) I versus q and (b) Lorentz corrected SAXS pattern of Iq^2 versus q, where I is the intensity and q is the scattering vector for blends of PA6/ABS with and without SMA modified MWNT (inset compares the Lorentz corrected SAXS patterns for PA6 and 20/80 PA6/ABS blends filled with 1 wt% MWNT).

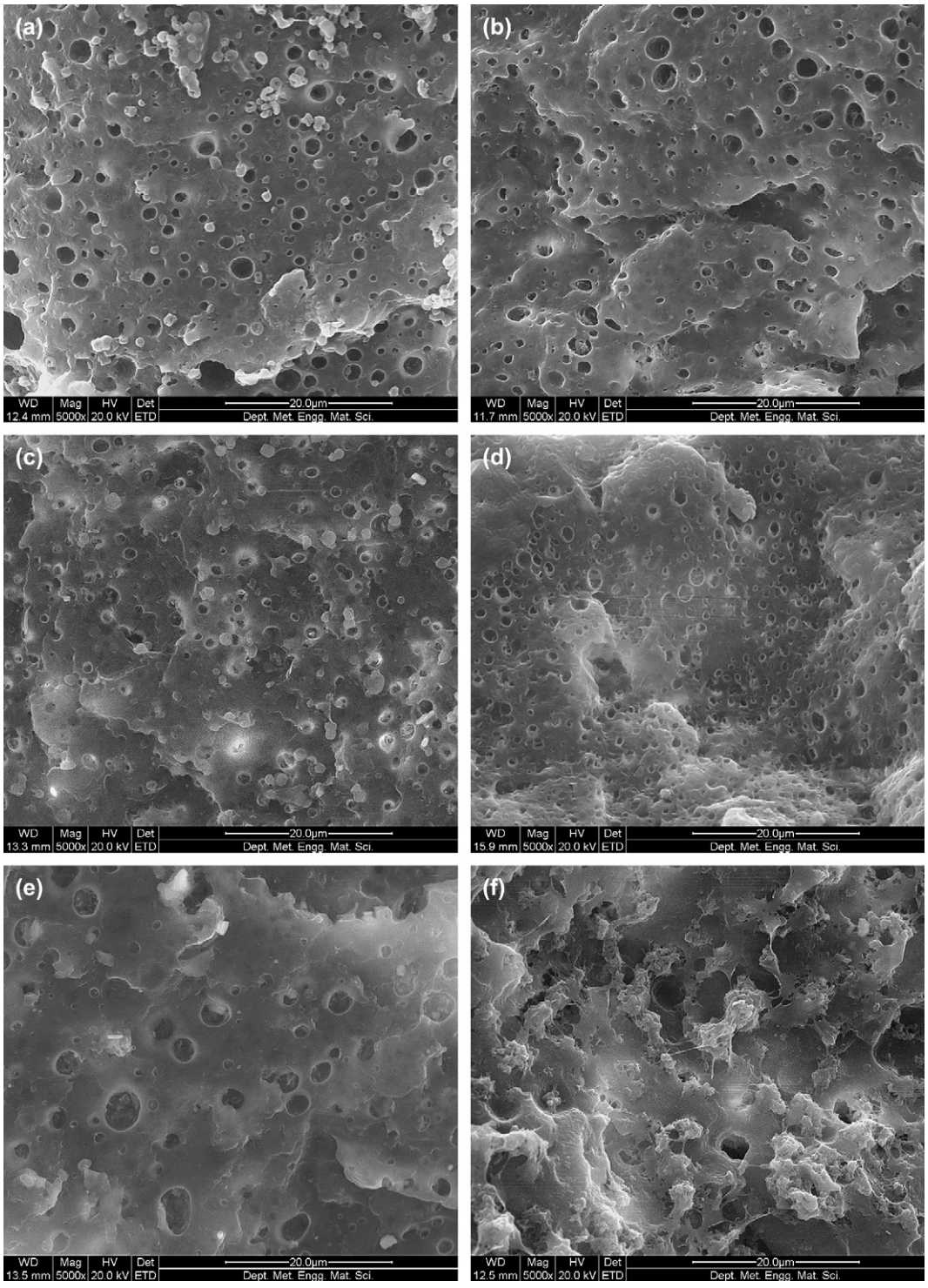

Fig. 4. SEM micrographs of (a) N20A80; (b) N20A80S2; (c) N20A80M0.5; (d) N20A80M1; (e) N20A80M2; (f) N20A80M5.

4. Conclusions

Crystallization of PA6 was strongly affected in the presence of ABS phase. We observed fractionated crystallization in melt-mixed blends of 20/80 PA6/ABS with or without SMA and SMA modified MWNT. Both the SMA and MWNT content were crucial in influencing the fractionated crystallization phenomenon of 20/80 PA6/ABS blends. Delayed crystallization was observed in uncompatibilized and SMA compatibilized blends. It is well evident that MWNT acted as a strong heterogeneity (nucleating) center in these set of blends manifested by an increase in the crystallization temperature. SAXS analysis revealed the formation of imperfect/thinner crystals arising from the multiple scattering

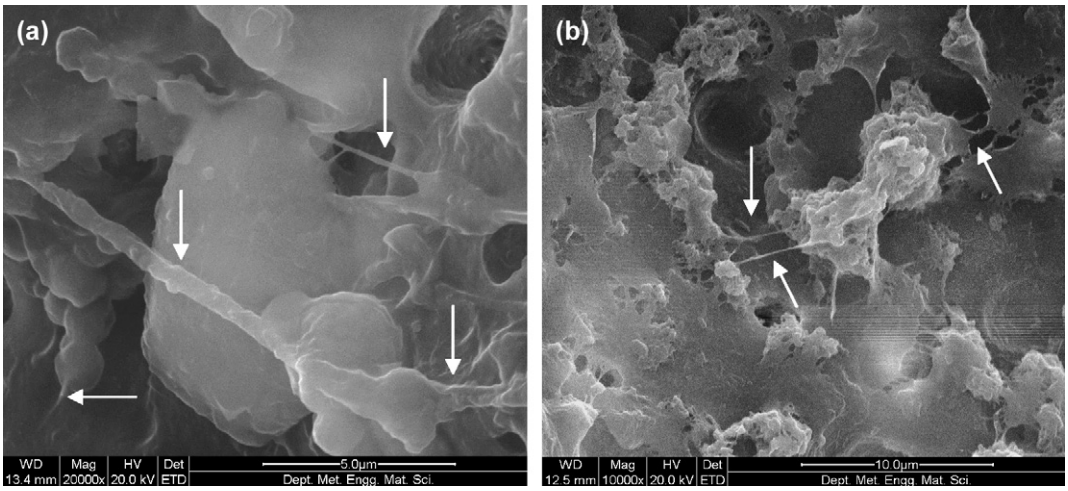

Fig. 5. SEM micrographs showing SMA encapsulated MWNT in (a) N20A80M0.5; (b) N20A80M5.

maxima. The encapsulating SMA layer on the MWNT surface hinders the nucleation and subsequent crystal growth from the heterogeneity site as would have been provided by the MWNT.

Acknowledgements

The authors duly acknowledge the financial support from the Department of Science and Technology (DST), India (SERC Fast Track Scheme, Project No. 04DS047). We thank Nova Chemicals, USA for providing the SMA copolymer used in this work. We would also like to acknowledge DST-FIST sponsored SAXS facility in the Chemical Engineering Department at IIT Bombay. We are grateful to Prof. Anil Kumar (Department of Chemistry, IIT Bombay) for providing DSC facility and to Dr. Vivek Pancholi (OIM-SEM National Facility, IIT Bombay) for assistance in SEM investigations.

References

[1] Turbull D. J Chem Phys 1950;18:198.
[2] Helfand E, Tagami Y. J Chem Phys 1972;56:3592.
[3] Frensch H, Harnischfeger P, Jungnickel B-J. In: Utracki L, Weiss RA, editors. Multiphase polymers: blends and ionomers. ACS Symposium Series, vol. 395; 1989. p. 101.
[4] Ikkala OT, Holsti-Miettinen RM, Seppälä J. J Appl Polym Sci 1993; 49:1165.
[5] Moon H-S, Ryoo B-K, Park J-K. J Polym Sci Polym Phys Ed 1994; B32:1427.
[6] Tang T, Huang B. J Appl Polym Sci 1994;53:355.
[7] Frensch H, Jungnickel B-J. Colloid Polym Sci 1989;267:16.
[8] Everaert V, Groeninckx G, Koch MHJ, Reynaers H. Polymer 1982; 23:1913.
[9] Zhang XQ, Son Y. J Appl Polym Sci 2003;89:2502.
[10] Wu Y, Yang Y, Li B, Han Y. J Appl Polym Sci 2006;100:3187.
[11] Yordanov Chr, Minkova L. Eur Polym J 2005;41:527.
[12] Tol RT, Mathot VBF, Groeninckx G. Polymer 2005;46:2955.
[13] Pompe G, Pötschke P, Pionteck J. J Appl Polym Sci 2002;86:3445.
[14] Haüßler L, Pompe G, Lehman D, Lappan U. Macromol Symp 2001; 164:411.
[15] Klemmer N, Jungnickel B-J. Colloid Polym Sci 1984;262:381.
[16] Tol RT, Mathot VBF, Groeninckx G. Polymer 2005;46:369.
[17] Androsch R, Stolp M, Radusch H-J. Thermochim Acta 1996;271:1.
[18] Shi D, Yin J, Ke Z, Gao Y, Li KYR. J Appl Polym Sci 2004;91:3742.
[19] Triacca VJ, Ziaee S, Barlow JW, Keskkula H, Paul DR. Polymer 1991;32:1401.
[20] Baer M. U.S. Patent 4,584,344 (assigned to Monsanto); 1986.
[21] Lavengood RE, Padwa RA, Harris AF. U.S. Patent 4,713,415 (assigned to Monsanto); 1987.
[22] Lavengood RE. U.S. Patent 4,777,211 (assigned to Monsanto); 1988.
[23] Iijima S. Nature 1991;354:56.
[24] Bhattacharyya AR, Sreekumar TV, Liu T, Kumar S, Ericson LM, Hauge RH, et al. Polymer 2003;44:2373.
[25] Valentini L, Biagiotti J, Kenny JM, Santucci S. J Appl Polym Sci 2003;87:708.
[26] Grady BP, Pompeo F, Shambaugh RL, Resasco DE. J Phys Chem B 2002;106:5852.
[27] Wu T-M, Chen E-C. J Polym Sci Part B Polym Phys 2006;44:598.
[28] Ryan KP, Cadek M, Drury A, Ruether M, Blau WJ, Coleman JN. Fullerenes Nanotubes Carbon Nanostruct 2005;13(Suppl. 1):431.
[29] Brandrup J, Immergut EH. Polymer handbook. 2nd ed. New York: Wiley; 1975.
[30] Turnbull D, Cech RE. J Appl Phys 1950;21:804.
[31] Galeski A, Bartezak Z, Pracella M. Polymer 1984;25:1323.
[32] Bartezak Z, Galeski A, Pracella M. Polymer 1986;27:537.
[33] Bartezak Z, Galeski A, Krasnikova NP. Polymer 1987;28:1627.